Mind the Gap: A Semicontinuum Model for Discrete Electrical Propagation in Cardiac Tissue

Caroline Mendonca Costa, Pedro Andre Arroyo Silva, and Rodrigo Weber dos Santos*

***Abstract*—Electrical propagation in cardiac tissue is a discrete or discontinuous phenomenon that reflects the complexity of the anatomical structures and their organization in the heart, such as myocytes, gap junctions, microvessels, and extracellular matrix, just to name a few. Discrete models or microscopic and discontinuous models are, so far, the best options to accurately study how structural properties of cardiac tissue influence electrical propagation. These models are, however, inappropriate in the context of large scale simulations, which have been traditionally performed by the use of continuum and macroscopic models, such as the monodomain and the bidomain models. However, continuum models may fail to reproduce many important physiological and physiopathological aspects of cardiac electrophysiology, for instance, those related to slow conduction. In this study, we develop a new mathematical model that combines characteristics of both continuum and discrete models. The new model was evaluated in scenarios of low gap-junctional coupling, where slow conduction is observed, and was able to reproduce conduction block, increase of the maximum upstroke velocity and of the repolarization dispersion. None of these features can be captured by continuum models. In addition, the model overcomes a great disadvantage of discrete models, as it allows variation of the spatial resolution within a certain range.**

***Index Terms*—Cardiac electrophysiology, discrete propagation, mathematical model, theoretical biophysics.**

I. Introduction

ALTHOUGH the idea of the myocardium being an assembly of discrete cells was established in the early 1950s [1], the effects of the structural discontinuities on electrical propagation were ignored, or at least set aside, for many decades. Thus, in general, activation was analyzed on the basis of continuum models (CMs), that consider the cardiac muscle as a syncytium. In the 1980s and 1990s, different researchers have introduced discrete models (DMs) [2], [3] or models with subcellular discretization and heterogeneous tissue conductivity [Fine-Mixed-Models (FMM)] [4]–[9] to study the effects of discontinuities in cardiac tissue. Their study suggested that changes in the propagation velocity, such as decreased conduction velocity (CV), and in action potential (AP) shape, such as increased maximal upstroke velocity (MUV), were strongly related to the gap-junctional resistance. These results were compared to experimental findings, as shown in [10], where a discontinuous cable model was able to reproduce experimental data. Their study supports the applicability of discontinuous models for describing longitudinal propagation in cardiac tissue. Later on, such results were related to conduction abnormalities, such as reentry, in the works of [11] and [12].

Recently, new studies that consider different microscopic aspects of cardiac tissue, such as fibroblast to myocyte interaction, and present 2-D or 3-D microscopic models [8], [9], [13]–[15] continue to use the FMM formulation, i.e., models with subcellular discretization and heterogeneous tissue conductivity. There are also recent studies that extend the 1-D DM formulation to 2-D and 3-D models [16], [17] to study the effects of randomly distributed conductivities in the CV and on the formation of reentry patterns.

These models, whether discrete or microscopic (with subcellular discretization), although accurate to study the effects of discontinuities are not appropriate in the context of large and complex geometries, where CMs, such as the monodomain and bidomain models, are largely employed [18], [19]. The main reason for that lies on the trusted independence of the continuum mathematical models with respect to the spatial domain, geometry, and mesh discretization. However, as pointed out by previous studies [3], [20], [21], for the case of low gap-junctional coupling, the aforementioned CMs fail to reproduce many aspects observed in the experiments. In addition, as we will show in this paper, the results obtained with continuum mathematical models are not independent of the mesh discretization.

In this study, we introduce a new model as a viable solution to fill this gap. We evaluate traditional CMs and DMs for the case of low gap-junctional coupling, where discrete propagation is observed, and present a novel hybrid semi-continuum model (SCM) that combines characteristics of both CMs and DMs. We call this new hybrid formulation an SCM as it is able to capture effects of discontinuous structures in propagation and it allows variation of the spatial resolution within a wide range.

II. Methods

A. Models for Electrical Propagation

1) CMs: The dynamics of the processes that underlie the AP in cardiac myocytes are typically described by a set of ordinary differential equations (ODEs) that describe the transmembrane current I_m:

$$I_m = C_m \frac{\partial V}{\partial t} + I_{\text{ion}}(V, \boldsymbol{\eta}) - I_{\text{stim}} \tag{1}$$

Manuscript received April 11, 2015; revised July 15, 2015; accepted August 7, 2015. Date of publication August 19, 2015; date of current version March 17, 2016. This work was supported by Brazilian grants from CNPq, CAPES, FINEP, UFJF, and FAPEMIG. *Asterisk indicates corresponding author.*

C. Mendonca Costa is with the Medical University of Graz.

P. A. Arroyo Silva is with the Federal University of Juiz de Fora.

*R. Weber dos Santos is with the Department of Computer Science and the Graduate Program of Computational Modeling, Federal University of Juiz de Fora, Juiz de Fora 36036-330, Brazil (e-mail: rodrigo.weber@ufjf.edu.br).

This paper has supplementary downloadable material available at http://ieeexplore.ieee.org (File size: 1 MB).

Digital Object Identifier 10.1109/TBME.2015.2470256

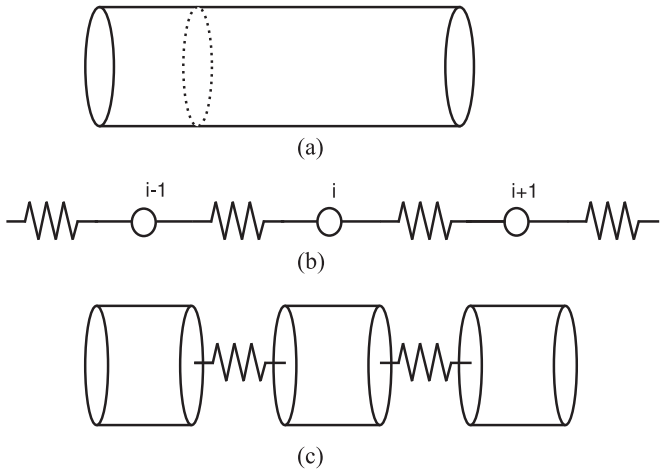

Fig. 1. Underlying geometries and structures of the (a) CM, (b) FMM, and (c) DM, where i is cell number.

$$\frac{d\boldsymbol{\eta}}{dt} = f(t, \boldsymbol{\eta}) \tag{2}$$

where C_m is the membrane capacitance, V is the transmembrane potential, I_{ion} is the density of the total ionic current, which depends on V and on a set of state variables $\boldsymbol{\eta}$, and I_{stim} is a stimulus current. In this study, we use the Luo–Rudy model as presented in [22] to describe the AP of mammalian ventricular myocytes.

In cardiac tissue (here we consider the 1-D case), the spread of excitation wave can be described by the monodomain formulation:

$$\beta I_m = \bar{\sigma} \partial_{xx} V \tag{3}$$

where $\bar{\sigma}$ is the homogenized conductivity and β is the homogenized membrane surface-to-volume ratio. Here, the homogenized conductivity is given by

$$\bar{\sigma} = \frac{\ell}{\frac{\ell}{\sigma_c} + \frac{A}{G}} \tag{4}$$

where ℓ is the length of the cell, σ_c is the conductivity in the cytoplasm, A is the area transverse to the cell, and G is the gap junction conductance. Fig. 1(a) shows the geometric idea behind CMs: cardiac tissue is considered as a continuous cable model.

2) FMM: The use of homogenized conductivity is based on the assumption that the effect of gap-junctional resistance is small enough that it can be averaged over the entire cell to give place to a uniform cable. It is already known that this assumption is not appropriate for the case of low gap-junctional coupling, where the gap-junctional resistance is too large to be ignored or averaged [3]. In such cases, a more appropriate description of cardiac activity is given by a heterogeneous, mixed, or hybrid versions of the monodomain model, in which different conductivities are employed for the cytoplasm and the gap junctions. This model is described by the equations below

$$\begin{aligned} \beta C_m \frac{\partial V(x,t)}{\partial t} + \beta I_{\text{ion}}\left(V(x,t), \boldsymbol{\eta}(x,t)\right) &= \partial_x\left(\sigma(x)\partial_x V\right) \\ \frac{\partial \boldsymbol{\eta}(x,t)}{\partial t} &= f\left(V(x,t), \boldsymbol{\eta}(x,t)\right) \end{aligned} \tag{5}$$

where V is the transmembrane potential, I_{ion} the total ionic current, which depends on V and a set of state variables $\boldsymbol{\eta}$, β is the surface-to-volume ratio, σ is the tissue conductivity which varies in space, and C_m is the membrane capacitance. Fig. 1(b) shows the geometric idea behind FMMs, as those used in [7], [9]; intracellular domain of myocytes is considered as a continuous cable model with a homogeneous cytoplasmic electric conductivity. However, the connections to neighboring myocytes are performed by discrete resistors that reflects the small dimension and high resistance of gap junctions.

3) DMs: In the case of low gap-junctional coupling, according to Keener in [3], the opposite assumption of the cable theory, that the gap-junctional resistance is more important than the cytoplasm resistance is worth exploring. This assumption leads to a DM, based on the monodomain model, that describes the electrical propagation in a 1-D cable of n cells. In this model, the cells are assumed to be isopotential and the cytoplasmic resistance insignificant. Thus, the model can be described by n systems of nonlinear ODEs:

$$\beta I_{m\,i} = \bar{\sigma}_D \Delta^2 V_i \tag{6}$$

where V_i with $i = 1$ is the transmembrane potential at each ith cell and $\Delta^2 V_i$ is the discrete operator $\Delta^2 V_i = \frac{V_{i-1} - 2V_i + V_{i+1}}{l^2}$.

The DM proposed in [3] takes $\bar{\sigma}_D = \frac{l}{A/G}$, i.e., it considers the cytoplasmic resistance $1/\sigma_c$ to be insignificant. We will show that the numerical solution of this DM that we call ODM, indeed approaches that of the FMM for the case of low gap-junctional coupling. However, it fails for the case of normal gap-junctional coupling, which is in agreement with the fact that in this case the cytoplasmic resistance cannot be considered insignificant.

Better results are obtained using another DM as proposed in [2], i.e., considering (6) with $\bar{\sigma}_D = \bar{\sigma}$ which is the same homogenized conductivity as given by (4). This model assumes that the individual cells are isopotential and the intercellular resistance includes both the cytoplasmic resistance and the resistance of the gap junctions between the cells. We call this DM the DM model. One may notice that considering a second-order finite difference approximation of the second derivative of V, in (3), i.e., $\partial^2 V(x) = \frac{V(x+\Delta x) - 2V(x) + V(x-\Delta x)}{\Delta x^2}$ the DM can be considered as a special case of the discretized CM, when $\Delta x = \ell$.

Fig. 1(c) shows the geometric idea behind DMs: cells are assumed to be isopotential and the connections to neighboring myocytes are performed by discrete resistors.

4) SCMs: We will show that the DM model accurately describes the electrical propagation for the case of low and normal gap-junctional coupling. However, it demands a perfectly correct and aligned spatial discretization with respect to the myocytes length and the distances between neighboring myocytes. One of the good features of CMs is that they do not depend on

the spatial domain, and their spatial discretization, or meshes, can be designed to match both the geometry of interest and the desired numerical accuracy of the solution. Therefore, in this study, we propose hybrid models, that combine characteristics of the CMs and the DMs.

We begin the deduction of the hybrid models by looking for a correction term Q for the CM that satisfies

$$\partial^2 V(x) + Q = \Delta^2 V \tag{7}$$

where $\Delta^2 V = \frac{V(x+\ell)-2V(x)+V(x-\ell)}{\ell^2}$ is the discrete operator defined in (6), and $\partial^2 V(x) = \frac{V(x+\Delta x)-2V(x)+V(x-\Delta x)}{\Delta x^2}$ is a second-order finite difference approximation of $\partial_{xx} V(x)$ that appears in the CM (3).

Therefore, we look for a correction term Q that approximates the CM to the discrete one. Expanding the terms $V(x+\ell)$, $V(x+\Delta x)$, $V(x-\ell)$, and $V(x-\Delta x)$ via Taylor series and truncating at the fourth-order term (see Supplementary material), we find that that the correction term we are looking for is given by

$$Q \approx \left(\frac{\ell^4 - \Delta x^4}{12\ell^2}\right) \frac{\partial^4 V(x)}{\partial x^4}.$$

Therefore, the discrete operator can be approximated by

$$\Delta^2 V \approx \partial_{xx} V(x) + \left(\frac{\ell^4 - \Delta x^4}{12\ell^2}\right) \partial_{xxxx} V(x). \tag{8}$$

Finally, replacing this approximation in (6), we find a fourth-order approximation of the DM given by the partial differential equation (PDE) below

$$\begin{aligned} \beta\left(C_m \partial_t V + I_{ion}(V, \boldsymbol{\eta})\right) &= \bar{\sigma}_D \partial_{xx} V + \bar{\sigma}_D \frac{\ell^4 - \Delta x^4}{12\ell^2} \partial_{xxxx} V \\ \partial_t \boldsymbol{\eta} &= f(V, \boldsymbol{\eta}). \end{aligned} \tag{9}$$

We call this model a SCM, since this can be viewed as a system of nonlinear PDE with constant coefficients, that depend on the discretization (Δx). This is the case of the coefficient that multiplies $\partial_{xxxx} V$: $\bar{\sigma}_D \frac{\ell^4 - \Delta x^4}{12\ell^2}$.

In the numerical methods and results section, we will show that the numerical discretization of the SCM model deduced above have some undesirable features: 1) The discretization of the fourth-order term involves a larger stencil (for 1-D, five points against the traditional three points). Therefore, the numerical scheme is computationally more expensive and more complex than those traditionally used for the monodomain equations. 2) The numerical solution of the SCM model presented some stability problems for the case considered in the numerical experiments.

To overcome these problems, we deduce another SCM by rearranging the terms of the Taylor series used to deduce (8) in a similar fashion to the method presented in [23]. It is well known that a Taylor expansion can often be accelerated by being rearranged into a ratio of two different expansions, called Padé Approximants [24]. Thus, using Padé Approximants instead of the Taylor expansion (see Supplementary material), we find a new approximation for the discrete operator:

$$\Delta^2 V \approx \frac{\partial_{xx}}{1 - \left(\frac{\ell^4 - \Delta x^4}{12\ell^2}\right) \partial_{xx}} V(x). \tag{10}$$

Replacing this new approximation in (6), we find another fourth-order approximation of the DM:

$$\begin{aligned} I_m &= \beta(C_m \partial_t V + I_{ion}(V, \boldsymbol{\eta})) = \bar{\sigma} \frac{\partial_{xx}}{1 - \frac{\ell^4 - dx^4}{12\ell^2} \partial_{xx}} V \\ \partial_t \boldsymbol{\eta} &= f(V, \boldsymbol{\eta}). \end{aligned} \tag{11}$$

We call this model a SCM based on a Padé approximation (SCMP).

B. Numerical Schemes

All models presented earlier in this study can be viewed as a coupled system of a parabolic PDE (or something that reminds the discretization of a PDE, in the case of DMs) and a set of nonlinear ODEs. An operator splitting was applied in this study to separate the PDE from the nonlinear ODEs

$$\begin{aligned} V^{k+\frac{1}{2}} &= -\Delta t I_{ion}(V^k, \boldsymbol{\eta}^k) + V^k \\ \boldsymbol{\eta}^{k+\frac{1}{2}} &= \Delta t f(V^k, \boldsymbol{\eta}^k) + \boldsymbol{\eta}^k \end{aligned} \tag{12}$$

$$V^{k+1} - V^{k+\frac{1}{2}} = \Delta t \frac{A}{B} V^{k+1}. \tag{13}$$

The set of nonlinear ODEs, (12), is solved via the Euler Explicit method, whereas, (13) with the Euler Implicit method. The operators A and B in (13) are defined by the chosen model and the spatial discretization method. In this study, we have used the finite volume method. In the case of FMM, CM, ODM, and DM, $B = I$ and A involves the discretization of the second-order derivative. For these models, A is a tridiagonal matrix. In the case of SCM, $B = I$ and A involves the discretization of both second-order and fourth-order derivatives. Therefore, for the SCM model, A is a pentadiagonal matrix. In the case of SCMP, both A and B involve the discretization of the second-order derivative, i.e., A and B are both tridiagonal matrices. Therefore, the SCMP model is computationally as complex and expensive as the discrete or CM. Further details of the numerical schemes are presented in the Supplementary material.

C. Simulation Setup

All models were simulated along a 1-D cable of 64 connected cells. A depolarizing current of $-80\,\mu$A/cm^2 was injected in the first 10% of discretization during 3.5 ms. The models were simulated for 12.6 ms, for 100% and 10% of gap-junctional coupling. Simulation time was set to 630 ms for the case of 1% of gap-junctional coupling. The values of the parameters used in the simulations are presented in Table I. These values are based on the study of [9].

D. Metrics

We compare the different models in terms of MUV, CV, action potential duration (APD), APD dispersion, and repolarization dispersion. The MUV is calculated as the maximum derivative

TABLE I
SIMULATION PARAMETERS

Parameter	Value
σ_c	4.0 mS/cm
G	$0.628\,\mu$S
A	$235.6\,\mu\text{m}^2$
$\bar{\sigma}$	1.5998 mS/cm
ℓ	0.0100 cm
C_m	$1.0\,\mu\text{F/cm}^2$
β	$1400.01/\text{ cm}^2$

of the AP at the center of a cell. For the case of the FMM model, we report the mean, maximum, and minimum MUV values observed within the central cell of the cable. CV is calculated between the four central cells of the cable, as the difference between the time where the MUV occurs in the 34th cell and 30th divided by the distance between these two cells. The APD is calculated as the difference between the time instant where 90% of repolarization is achieved and the time instant where the MUV occurs. APD dispersion is calculated as difference between the maximum and minimum APDs along the cable, whereas the repolarization dispersion is calculated as the difference between the time instants where the maximum and minimum repolarization time instants occur. In addition, the percentage relative errors of CV, MUV, APD, and repolarization dispersions were calculated as $err = \frac{\|obj-appr\|_2}{\|obj\|_2}$, where obj is the given metric obtained with the FMM, our gold standard, and $appr$ is the same metric obtained with CM, SCM, or SCMP.

III. RESULTS

Cardiac arrhythmia is known to be strongly related to membrane properties, such as MUV and refractory period. Therefore, we evaluate how the models behave in terms of such features when gap-junctional coupling is reduced. We split the results into two sections: results obtained with the DMs (ODM, DM) are compared to those obtained by the CMs (FMM) that use very fine spatial discretization ($0.5\,\mu m$); and results obtained with the SCMs (SCM, SCMP) are compared to those obtained by the CMs (FMM) using different values for the spatial discretization. We further split the two sections according to the feature: depolarization (CV, MUV, and AP shape) and repolarization (APD and repolarization dispersion).

A. CMs Versus DMs

1) Depolarization: Fig. 2 shows the CV of the FMM, CM, ODM, and DM models for the cases of different gap-junctional coupling. Similarly to [6], CV decreases as the level of gap-junctional coupling decreases for all models. However, when using the FMM or the DMs, propagation fails for gap-junctional coupling values lower than 0.56%, whereas when using the CM propagation persists. In particular, for gap-junctional coupling reduced to 1% of its normal value CV is around 3.85 cm/s for the FMM and the DMs, but it is about twice as fast with the CM. For normal gap-junctional coupling 100%, the ODM fails to reproduce the CV of the FMM. In this case, CV is around

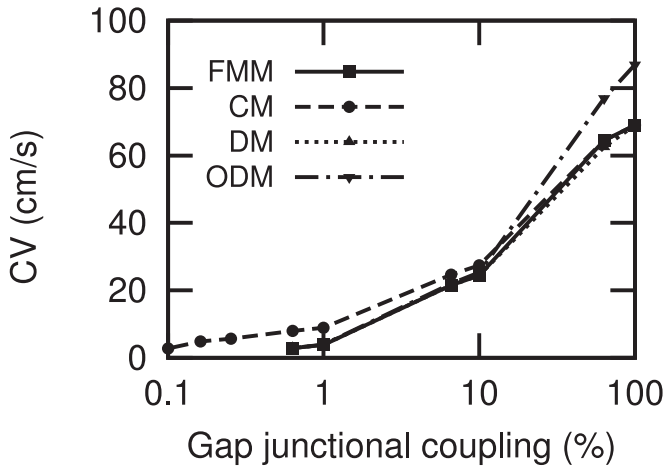

Fig. 2. Longitudinal CV of the FMM, CM, and DM models for different values of gap-junctional coupling.

69 cm/s when using the FMM model and 87 cm/s when using the ODM model. Therefore, in terms of CV, DM is the model that best approximates the FMM model for simulations using different values of gap-junctional coupling. For this reason, the ODM model will not be included in the next results, and we will only compare CM, DM, and FMM.

Fig. 3 shows the depolarization phase of APs obtained from the central cell of the cable when using the FMM, CM, and DM for 100%, 10%, and 1% of gap-junctional coupling. For normal gap-junctional coupling, 100%, the APs of the three models are very similar in shape and time of depolarization. However, for reduced coupling, the AP obtained with CM differs greatly from the AP obtained with FMM and DM. Particularly, for 1% of gap-junctional coupling, the AP obtained with the FMM and DM rises in clusters, whereas for the CM depolarization is monotonic.

Fig. 4 shows the MUV for different coupling conditions. Also similarly to [6], using the FMM, MUV increases from ~ 223 to ~ 379 mV/ms as the gap-junctional coupling is reduced to 1%. The DM closely reproduces this behavior, whereas the CM fails by not exhibiting any variation of the MUV for different values of gap-junctional coupling, i.e., it is equal to 230 mV/ms for all coupling conditions.

In summary, when compared to the FMM in terms of CV, AP shape, and MUV, the CM failed by: 1) not reproducing propagation failure when coupling in reduced, 2) generating CV values twice greater than the correct ones, 3) not reproducing the correct AP shape during depolarization, 4) not reproducing the known dependence between MUV and gap-junctional coupling [25]. On the other hand, the DM was able to closely reproduce these four behaviors.

2) Repolarization: Fig. 5 presents the results for APD and repolarization dispersions along the cable obtained with the FMM, CM, and DM for 100%, 10%, and 1% of gap-junctional coupling. The continuum monodomain model CM fails to reproduce both APD dispersion and repolarization dispersion for the case of 1% of gap-junctional coupling. In this case, FMM and DM obtained a value for APD dispersion near 13 ms, whereas

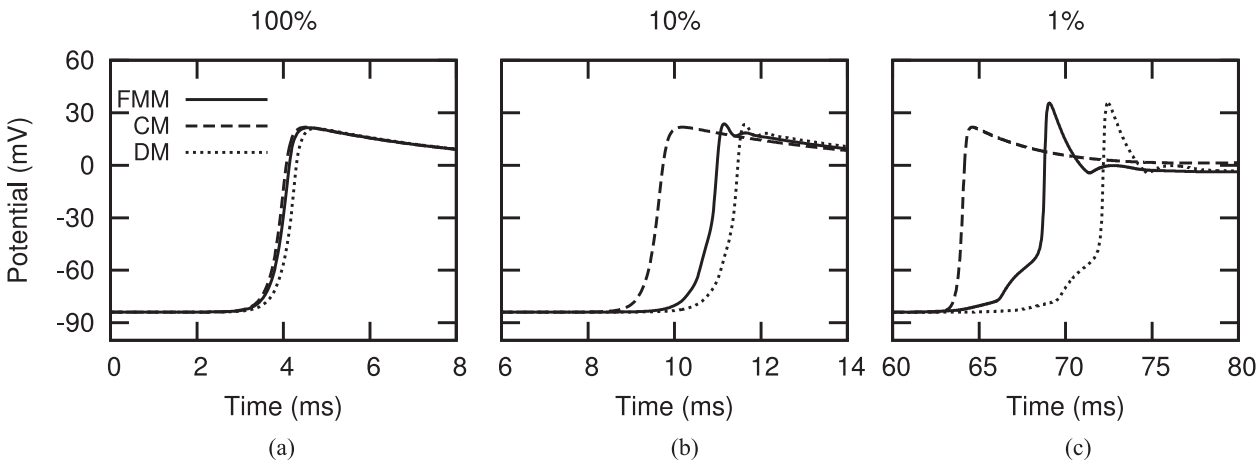

Fig. 3. AP depolarization phase of the FMM, CM, and DM models for 100%, 10%, and 1% of gap-junctional coupling. For 1%, the AP of the CM was shifted forward 35 ms in time, to aid visualization.

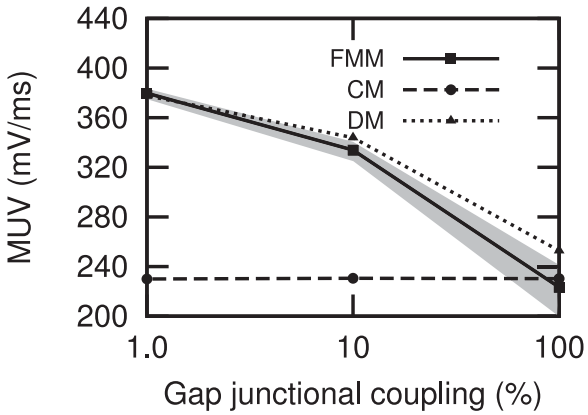

Fig. 4. MUV obtained with the FMM, CM, and DM for 100%, 10%, and 1% of gap-junctional coupling. For the FMM the central value is the mean value of MUV and the shaded area represents maximum and minimum MUV values observed within the central cell of the cable.

the CM value is 8 ms. FMM and DM value for repolarization dispersion is around 141 ms, whereas the CM value is 63 ms, i.e., less than half of the correct one.

B. CMs Versus SCMs

We now evaluate the proposed SCMs, SCM, and SCMP, as well as the CM, by presenting the errors of each metric relative to the FMM for different gap-junctional couplings and different values for spatial discretization.

1) Depolarization: Fig. 6 shows the CV errors for the CM, SCM, and SCMP relative to the FMM for different gap-junctional coupling values as the spatial discretization varies. For normal coupling, the models do not show significant dependence on discretization, exhibiting errors around 5%. However, with reduced gap-junctional coupling, particularly for the extreme case of 1%, the models exhibit a similar behavior only for $\Delta x = 100\,\mu$m. The errors and differences increase for the discretization values smaller and larger than $100\,\mu$m. For 1% of gap-junctional coupling, the CM produces the highest error values, since the error increases from $\sim 0\%$ to $\sim 131\%$ as the spatial discretization size decreases from 100 to $1\,\mu$m. The SCM produces much smaller errors, but it is shown to be conditionally stable as it does not allow the use of spatial discretizations smaller than $55\,\mu$m. Therefore, the SCM model will not be included in the next results. In contrast, the SCMP always produces smaller error values than the CM (less than $\sim 35\%$ in the worst case) and it allows the use of a wider range of spatial discretizations. In this figure as well as in the following figures, we mark with "X" any result that already presents oscillations due to instability issues.

Another important limitation of the CM model is observed for the case of reduced gap-junctional coupling (at 1%): for spatial discretizations larger than $115\,\mu$m propagation block is observed (see Fig. 6), whereas the correct value of CV given by the FMM and DM is around 4 cm/s (see Fig. 2). This artificial propagation block is well known to occur for numerical discretizations of the monodomain model as already described in [3]. In this figure as well as in the following figures, we mark with a square any result that is associated with an artificial propagation block. For the SCMP model, this artificial propagation block was never observed. Nevertheless, the numerical discretization used for the SCMP model in this study is conditionally stable (CFL conditions are derived in the Supplementary material). In particular, for the case of 1% of gap-junction coupling, the numerical method used for SCMP was found to be stable for $\Delta x < 180\,\mu$m (for the parameters used in this study, see Table I).

Fig. 7 shows that the SCMP model also outperforms the CM in terms of predicted value for gap junction coupling where conduction block occurs. Using the SCMP model, we observe conduction block at a value of 0.9% of gap-junctional coupling. The values obtained by the CM and FMM models are 1.8% and 0.6%, respectively.

Fig. 8 presents the errors of MUV relative to the FMM with various spatial discretizations, for 100%, 10%, and 1% of gap-junctional coupling. MUV errors are always below 13% for the SCMP model, whereas the errors are as high as 35% when using

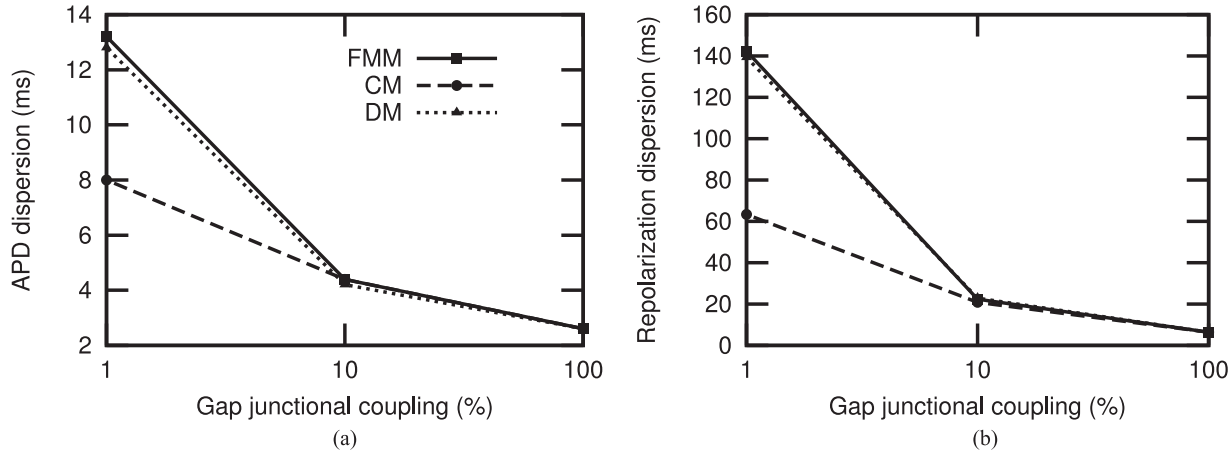

Fig. 5. APD and repolarization dispersions obtained with the FMM, CM, and DM for 100%, 10%, and 1% of gap-junctional coupling.

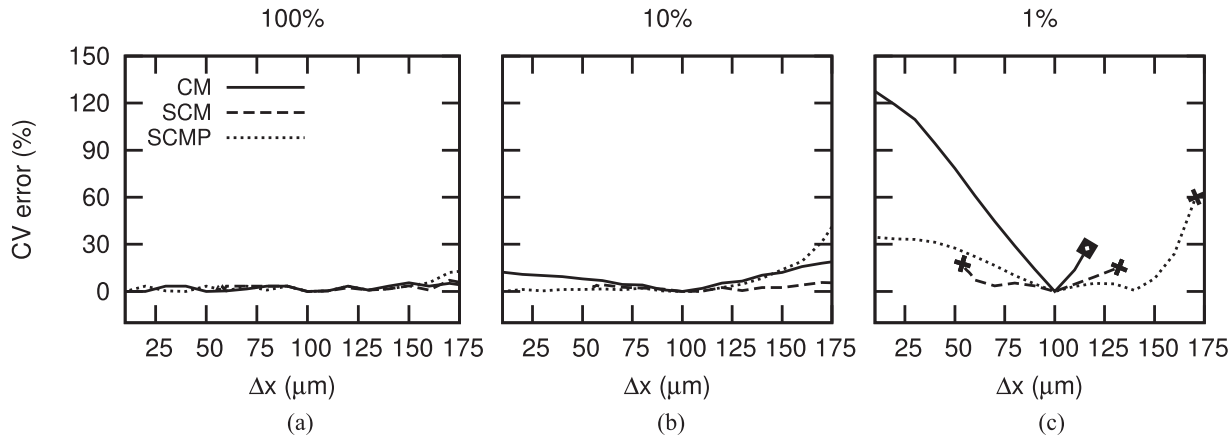

Fig. 6. CV error of the SCMP, SCM, and CM compared to the FMM. Results are for various values of Δx and for 100%, 10%, and 1% of gap-junctional coupling.

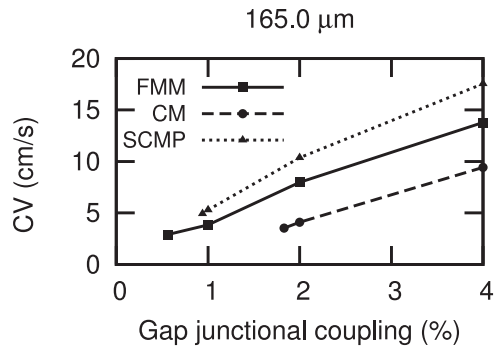

Fig. 7. CV of the FMM, CM, and SCMP, results are for $\Delta x = 165.0\,\mu$m for different values of gap-junctional coupling.

CM. It is worth noting that for this particular metric (MUV), these errors were observed for all values of gap-junctional coupling tested (100%, 10%, and 1%), i.e., not only for the case of low gap-junctional coupling.

2) Repolarization: Fig. 9 presents the errors of APD and repolarization dispersions relative to the FMM with various spatial discretizations, for the case of 1% of gap-junctional coupling. For the other cases of gap-junctional coupling (100% and 10%), the errors obtained by both CM and SCMP were similar. As presented in Fig. 9, APD and repolarization dispersion errors are always below 24% for the SCMP model, whereas these errors are as high as 55% when using the CM.

IV. Discussion

The underlying mechanisms of cardiac arrhythmia are known to be strongly related to the length of the propagating wave [26], which in turn depends on membrane properties, such as MUV and refractory period, as well as CV. CV is influenced by both MUV and conductivity values, and the refractory period is influenced by the dispersion of APD and repolarization. In this study, discrete propagation was studied via different scenarios of low gap-junctional coupling.

Different mathematical models were compared using, as reference, a microscopic version of the classical monodomain model with subcellular discretization and heterogeneous conductivity. Our results show that for the case of low gap-junctional coupling, the CM fails to reproduce AP characteristics during the depolarization and repolarization phases. Such characteristics

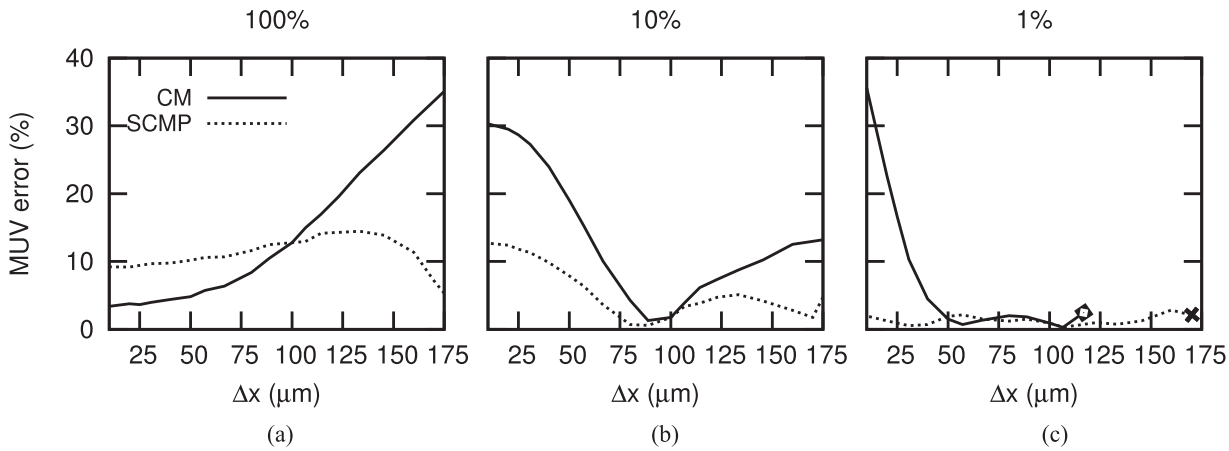

Fig. 8. MUV error of the SCMP, SCM, and CM compared to the mean value obtained with the FMM. Results are shown for various values of Δx and for 100%, 10%, and 1% of gap-junctional coupling.

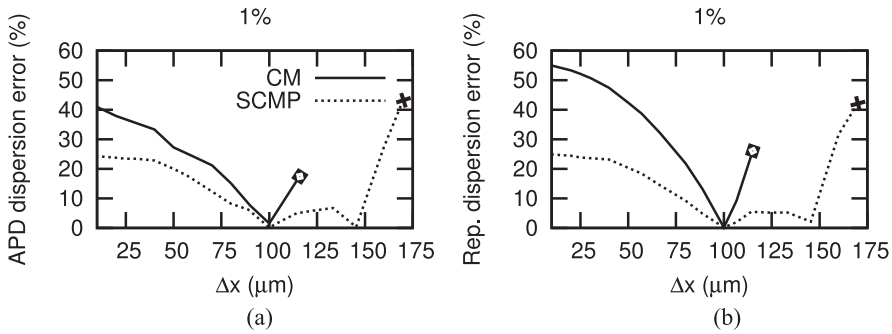

Fig. 9. Repolarization dispersion error of the SCMP, SCM, and CM compared to the FMM. Results are shown for different values of Δx and for 1% of gap-junctional coupling.

are, however, well reproduced by DMs here investigated. On the other hand, the DM is not appropriate in the context of complex geometries, as it requires the spatial discretization to be fixed and correctly aligned with every myocyte location. The heterogeneous CM is also not appropriate in this context, since it requires very fine spatial discretizations.

To overcome the aforementioned limitations of CMs or DMs in the case of low gap-junctional coupling, we deduce and investigate two new hybrid models. These hybrid models or SCMs aim to combine the advantages of both CMs and DMs, i.e., to be independent of the chosen spatial discretization (to some extent) and to accurately reproduce electrophysiological features associated with discrete propagation.

The first SCM we have introduced has produced results with much smaller errors in CV ($\approx 14\%$) than those obtained by the CM ($\approx 127\%$). However, the model was shown to be conditionally stable as it did not allow the use of spatial discretizations smaller than $55\ \mu$m. In addition, the numerical solution of this model requires the solution of a pentadiagonal matrix, which increases its complexity and computational cost. Therefore, this model is also not appropriate for complex geometries.

On the other hand, our results show that the SCMP reproduced very well the propagation features in cardiac tissue during low gap-junctional coupling. Particularly, in terms of CV, the errors were below 35% for all tested spatial discretizations. Similar results were observed for the MUV, and the dispersion of APD and repolarization. Therefore, the SCMP was able to reproduce most of the phenomena associated with discrete propagation (overcoming the drawbacks of a CM) and it allows the use of different spatial discretizations within a wide range (overcoming the drawbacks of a DM). In addition, the numerical solution of the SCMP is obtained via the solution of a linear system based on a tridiagonal matrix, i.e., its computational complexity is equivalent to that of a CMs or DM.

It is worth mentioning that the scenarios of low gap-junctional coupling were adopted as a theoretical tool to generate a framework of discrete propagation. As mentioned before, gap junctions are strongly associated with discrete propagation both in physiological (for instance, in the atrioventricular node [27]) and pathophysiological conditions (for instance, in acute ischemia, ventricular hypertrophy, heart failure, and myocarditis [28], [29]). Nevertheless, other structures of cardiac tissue contribute to discrete propagation, such as microvasculature, connective tissue, extracellular matrix, and cleft spaces. Therefore, we understand that our proposed SCM is an alternative formulation that can be adjusted to describe different cases of discrete propagation, i.e., it is not limited to the case of low gap-junctional coupling.

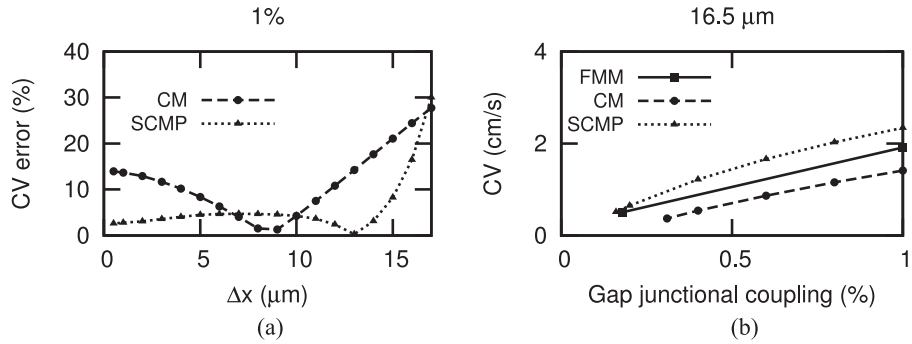

Fig. 10. (a) Transverse CV errors of the CM and SCMP compared to the FMM, results are shown for different values of Δx and for 1% of gap-junctional coupling. (b) Transverse CV of the FMM, CM, and SCMP, results are for $\Delta x = 16.5\,\mu$m.

A. CV and Repolarization Wave

Our results have shown that the DM and SCMP models captured repolarization and APD dispersion more accurately than the traditional CM model. In fact, repolarization and APD dispersion errors presented in Fig. 5 can be related to errors in capturing the phenomenon called electrotonic effect [30], [31]. Fig. 5 shows that the electrotonic effect is overestimated by the CM for the case of low gap-junctional coupling. Regardless of the different ways, this particular phenomenon can be explained, it can certainly be related to what is also called repolarization wave [32]. Therefore, dispersion of APD and of repolarization is small if the "information of repolarization" propagates fast in the tissue and vice-versa. Therefore, Fig. 5 suggests that the CM model overestimates the speed of the repolarization wave. This is also in agreement with what happens in terms of speed of depolarization, or CV. Fig. 2 shows that, indeed, the CM model also overestimates CV for the case of low gap-junctional coupling.

B. Transverse Propagation and 3-D Extension of SCMP

In this section, we speculate on the performance of an extension of the presented SCMP model to the case of 3-D simulations. We begin with an analysis for the case of 1-D transverse propagation, by setting $l = 10\,\mu$m and $\bar{\sigma} = 0.1538462\,$mS. First, an analytic investigation was performed in the supplemental material. If we consider the case of very low gap-junction coupling ($\bar{\sigma}$ near zero), we can simplify the CFL condition of the numerical method used in this study and find that: $\Delta x < 1.82\ell$. As shown in Fig. 6, the CM model only presents a similar accuracy to the SCMP model when Δx is very close to ℓ. Therefore, in 1-D simulations, the SCMP model could use near-half discretization points than the CM model (or the DM model, which is the case $\Delta x = \ell$) for whatever the case of fiber alignment (transverse or longitudinal) for $\bar{\sigma}$ near zero.

Numerically, we have also performed simulations for the case of transverse propagation. Fig. 10(a) presents how the CV error of the CM and SCMP models varies (as compared to the FMM model) with Δx, for the case of gap-junction coupling reduced to 1% of its normal value. Different from the results for longitudinal propagation presented in Fig. 6, both models behave qualitatively similar and present errors around 30% for Δx near 20 μm. Also different from the previous case, we have not observed any artificial block using the CM model nor instability issues for the SCMP model. The explanation for this different behavior can be found in Fig. 10(b) that presents how CV varies for different values of gap-junction coupling for the CM, SCMP, and FMM. From Fig. 10(b), we observe that for transverse fibers, propagation blocks at much lower values for gap-junctional coupling. The FMM model presents propagation block at 0.18%. This is the reason why at 1% the CM and SCMP performances are similar. Fig 10(a) (transverse case) would be equivalent to Fig. 6(b) (longitudinal case). Nevertheless, as also presented in Fig. 10(b) the SCMP model outperforms the CM model in terms of the predicted value for propagation block, 0.16% versus 0.31%, respectively.

Using the results above, we can speculate about the performance of an extension of the SCMP model for 3-D simulations. If we take a 3-D mesh that was generated without the information of fiber direction, its volume or element edges should not vary notably and is usually close to a parameter Δx that was set by the user during mesh generation. In this scenario, if we use the extended SCMP 3-D model with Δx near $20\,\mu$m, we would expect CV errors around 30% for the case of 1% of gap-junctional coupling. This is the error indicated by Figs. 6(c) and 10(a) for the SCMP model with Δx near $20\,\mu$m. However, if we use the CM model on the same 3-D mesh the CV errors could be larger than 100% (see Fig. 6(c), CM model with Δx near $20\,\mu$m). Therefore, although the computational costs of CM and SCMP would be the same for this 3-D case (same numbers of nodes, volumes or elements), the SCMP would provide more accurate results.

On another scenario, imagine that our mesh generator can take into account cell's position and direction. It is clear from our results and discussion so far that a very good choice for model would be the DM. This would be equivalent to have mesh volumes of the size of a cell, for instance, $100 \times 10 \times 10$ μm^3. If, now, we use the extended SCMP model with volumes near $200 \times 20 \times 20$ we would expect CV errors around 30% for the case of 1% of gap-junctional coupling. This is the error of the SCMP model indicated by Fig. 6(c) (with Δx near $200\,\mu$m) and Fig. 10(a) (Δx near $20\,\mu$m). Therefore, theoretically an extension of the SCMP model to 3-D would need 2^3 less nodes (volumes or elements) than the DM. This would mean eight

times less memory and at least eight times faster simulations than those obtained with the DM model. It is worth noting that for this size of volume $200 \times 20 \times 20$ the CM model suffers from artificial propagation block as indicated by Fig 6(c) (CM with Δx near $200\,\mu$m).

V. Limitations and Future Studies

As a natural future study, we will propose extensions of our SCM for the cases of: heterogeneous conductivities, i.e., to consider also that the conductivity can vary in space, 2-D and 3-D geometries. However, before we proceed in this direction, we observe an immediate application of our 1-D SCM. In [33] and [34], the Purkinje system was modeled as a 1-D model embedded in a 3-D complex geometry. In addition, in [33], a modified version of the 1-D monodomain model was implemented, in which the conductivities were rescaled depending on the size of the finite element used. It seems that the rescaling was necessary due to the spatial discretization dependence inherited from the use of a CM, a drawback that was extensively studied in our study. Therefore, it is worth exploring the benefits of using our SCM to better describe propagation in the Purkinje system.

Our model can also be extended toward a bidomain model. In particular, the effect of extracellular cleft spaces in the case of discrete propagation during low gap-junctional coupling, as studied in [7], could be incorporated into our SCM. In the previously mentioned study, the authors show that at low gap-junctional couplings, ephaptic coupling increases AP propagation speed and can even prevent conduction failure. To describe such phenomenon, Hand and Griffith [35], [36] use the homogenization technique to derive a new bidomain model that considers the cleft spaces and is embedded in a multiscale modeling scheme. Alternatively, an SCM for the extracellular space, that considers the cleft space as the underlying discrete structure associated with ephaptic coupling, could be derived in a similar fashion as performed in this study, where the underlying discontinuous structure was the gap junction.

It is important to highlight that in this paper, we have deduced and proposed a new hybrid model for discrete propagation in cardiac tissue and also a first numerical implementation for it. All the results presented in this paper are directly affected by the current limitations of the numerical method implemented. Therefore, when we report that the error for CV at 1% of gap-junctional coupling is below 35% for the SCMP model, we should actually read that this error is related to the current numerical implementation of the SCMP model. Although a CV error of 35% is much better than 130% (this one obtained by a classical implementation of the traditional CM model), we acknowledge that this error may still be high for some applications. However, we believe the SCMP model can perform even better by using more appropriate numerical methods. For instance, the SCMP may have missed some important nonlinear effects due to the use of the operator splitting technique. This may have accidentally deteriorated the performance of the SCMP model. As an ongoing work, we are currently implementing a semi-implicit numerical method that does not use the operator splitting technique. Another clear limitation of the numerical method for the SCMP model is its CFL condition. We are also trying different discretizations in order to relax the current CFL condition and allow the SCMP model to use even larger spatial discretizations.

VI. Conclusion

In this study, we derived and evaluated a new mathematical model that captures the effects of discrete propagation in cardiac tissue. The new model lies in between classical CMs and DMs. The presented results suggest that this novel SCM is able to accurately describe characteristics of discrete propagation in cardiac tissue that cannot be captured by CMs. In addition, the new proposed model overcomes a great limitation of DMs, since it allows a wide range of choice of the spatial discretization. Finally, the computational complexity of the proposed model is equivalent to that of a continuum or DM. Therefore, we conclude that the newly introduced mathematical model has a great potential and can further contribute to the better comprehension of important aspects of cardiac biophysics.

References

[1] F. Sjostrand and E. Andersson, "Electron microscopy of the intercalated disc of cardiac muscle tissue," *Experientia*, vol. 10, pp. 36–370, 1954.

[2] R. Joyner, "Effects of the discrete pattern of electrical coupling on propagation through an electrical syncytium," *Circ. Res.*, vol. 50, pp. 192–200, 1982.

[3] J. Keener, "The effects of gap junctions on propagation in myocardium: A modified cable theory," *Ann. New York Acad. Sci.*, vol. 591, pp. 257–277, 1990.

[4] Y. Rudy and W. Quan, "A model study of the effects of the discrete cellular structure on electrical propagation in cardiac tissue," *Circ. Res.*, vol. 61, pp. 815–823, 1987.

[5] M. S. Spach and J. F. Heidlage. (1995). The stochastic nature of cardiac propagation at a microscopic level. *Circ. Res*. [Online]. Available: http://circres.ahajournals.org/content/76/3/366.full

[6] R. M. Shaw and Y. Rudy. (1997). Ionic mechanisms of propagation in cardiac tissue. *Circ. Res.* [Online]. *81(5)*, pp. 727–741. Available: http://circres.ahajournals.org/content/81/5/727.abstract

[7] J. Kucera *et al.*, "Localization of sodium channels in intercalated disks modulates cardiac conduction," *Circ. Res.*, vol. 91, no. 12, pp. 1176–1182, 2002.

[8] V. Jacquemet and C. S. Henriquez. (May 2008). Loading effect of fibroblast-myocyte coupling on resting potential, impulse propagation, and repolarization: Insights from a microstructure model. *Amer. J. Physiol. - Heart Circulatory Physiol.* [Online]. *294(5)*, pp. H2040–H2052. Available: http://ajpheart.physiology.org/content/294/5/H2040.abstract

[9] B. G. de Barros *et al.*, "Simulations of complex and microscopic models of cardiac electrophysiology powered by multi-GPU platforms," *Comput. Math. Methods Med.*, vol. 2012, art. no. 824569 (13 pages), 2012.

[10] W. Cole *et al.*, "Gap junctional uncoupling and discontinuous propagation in the heart," *Biophys. J.*, vol. 53, pp. 809–818, 1988.

[11] P. Ursell *et al.*, "Structural and electrophysiological changes in the epicardial border zone of canine myocardial infarcts during infarct healing," *Circ. Res.*, vol. 56, pp. 436–452, 1985.

[12] M. Spach and P. Dolber, "Relating extracellular potentials and their derivatives to anisotropic propagation at a microscopic level in human cardiac muscle: Evidence for electrical uncoupling of side-to-side fiber connections with increasing age," *Circ. Res.*, vol. 58, pp. 356–371, 1986.

[13] M. L. Hubbard *et al.*, "Effect of gap junction distribution on impulse propagation in a monolayer of myocytes: A model study," *Europace*, vol. 9, no. suppl 6, pp. vi20–vi28, 2007.

[14] J. Stinstra *et al.* (2010). Incorporating histology into a 3D microscopic computer model of myocardium to study propagation at a cellular level. *Ann. Biomed. Eng.* [Online]. *38*, pp. 1399–1414. Available: http://dx.doi.org/10.1007/s10439-009-9883-y

[15] S. F. Roberts *et al.*, "Effect of nonuniform interstitial space properties on impulse propagation: A discrete multidomain model," *Biophys. J.*, vol. 95, no. 8, pp. 3724–3737, 2008.
[16] S. Alonso *et al.* (2011). Effects of reduced discrete coupling on filament tension in excitable media. *Chaos: An Interdisciplinary J. Nonlinear Sci*. [Online]. *21(1)* p. 013118. Available: http://link.aip.org/link/?CHA/21/013118/1
[17] S. Alonso *et al.* (2012). Negative tension of scroll wave filaments and turbulence in three-dimensional excitable media and application in cardiac dynamics. *Bulletin Math. Biol*. [Online]. pp. 1–26. Available: http://dx.doi.org/10.1007/s11538-012-9748-7
[18] B. Rocha *et al.*, "A macro finite element formulation for cardiac electrophysiology simulations using hybrid unstructured grids," *IEEE Trans. Biomed. Eng.*, vol. 58, no. 4, pp. 1055–1065, Aug. 2010.
[19] D. Hooks *et al.*, "Cardiac microstructure: Implications for electrical propagation and defibrillation in the heart," *Circ. Res.*, vol. 91, no. 4, pp. 331–338, 2002.
[20] C. Mendona Costa and R. Weber dos Santos, "Limitations of the homogenized cardiac monodomain model for the case of low gap junctional coupling," in *Proc. IEEE Conf. Eng. Med. Biol. Soc.*, 2010, pp. 228–31.
[21] J. Stinstra *et al.*, "Comparison of microscopic and bidomain models of anisotropic conduction," in *Proc. Comput. Cardiol.*, Sep. 13–16, 2009, pp. 657–660.
[22] C. Luo and Y. Rudy, "A model of the ventricular cardiac action potential. Depolarization, repolarization, and their interaction," *Ann. New York Acad. Sci.*, vol. 591, pp. 257–277, 1990.
[23] P. Kevrekidis *et al.* (2002). Continuum approach to discreteness. *Phys. Rev. E. 65* [Online]. p. 046613. Available: http://link.aps.org/doi/10.1103/PhysRevE.65.046613
[24] G. A. J. Baker, *Essentials of Pade Approximants*. New York, NY, USA: Academic, 1975.
[25] A. Kléber and Y. Rudy. (2004). Basic mechanisms of cardiac impulse propagation and associated arrhythmias. *Physiol. Rev.* [Online]. *84(2)*, pp. 431–488. Available: http://physrev.physiology.org/content/84/2/431.abstract
[26] J. L. Smeets *et al.*, "The wavelength of the cardiac impulse and reentrant arrhythmias in isolated rabbit atrium. the role of heart rate, autonomic transmitters, temperature, and potassium," *Circ. Res.*, vol. 58, pp. 96–108, 1986.
[27] M. A. McGuire *et al.* (1996). Atrioventricular junctional tissue: Discrepancy between histological and electrophysiological characteristics. *Circulation*. [Online]. *94(3)*, pp. 571–577. Available: http://circ.ahajournals.org/content/94/3/571.abstract
[28] S. Kostin *et al.*, "Gap junction remodeling and altered connexin43 expression in the failing human heart," *Prog. Biophys. Mol. Biol.*, vol. 242, pp. 135–144, 2003.
[29] N. J. Severs *et al.*, "Remodelling of gap junctions and connexin expression in diseased myocardium," *Cardiovascular Res.*, vol. 80, no. 1, pp. 9–19, 2008.
[30] R. W. Dos Santos *et al.* (2006). Atx-ii effects on the apparent location of m cells in a computational model of a human left ventricular wedge. *J. Cardiovascular Electrophysiol. 17* [Online]. pp. S86–S95. Available: http://dx.doi.org/10.1111/j.1540-8167.2006.00389.x
[31] R. Weber dos Santos *et al.*, "Experimental and theoretical ventricular electrograms and their relation to electrophysiological gradients in the adult rat heart," *Amer. J. Physiol.-Heart Circulatory Physiol.*, vol. 297, no. 4, pp. H1521–H1534, 2009.
[32] V. M. Meijborg *et al.* (2014). Electrocardiographic t wave and its relation with ventricular repolarization along major anatomical axes. *Circulation: Arrhythmia Electrophysiol*. [Online]. *7(3)*, pp. 524–531. Available: http://circep.ahajournals.org/content/7/3/524.abstract
[33] M. Deo *et al.*, "The statistics of calcium-mediated focal excitations on a one-dimensional cable," *Amer. J. Physiol. Heart Circ. Physiol.*, vol. 102, no. 3, pp. 461–471, 2009.
[34] E. Cherry and F. Fenton, " Contribution of the purkinje network to wave propagation in the canine ventricle: Insights from a combined electrophysiological-anatomical model," *Nonlinear Dyn.*, vol. 68, no. 3, pp. 365–379, 2012.
[35] P. Hand and B. Griffith, "Adaptive multiscale model for simulating cardiac conduction," *Proc. Nat. Acad. Sci. USA*, vol. 107, pp. 14603–14608, 2010.
[36] P. Hand and C. Peskin, "Homogenization of an electrophysiological model for a strand of cardiac myocytes with gap-junctional and electric-field coupling," *Bull Math. Biol.*, vol. 72, no. 6, pp. 1408–1424, 2010.

Authors' photographs and biographies not available at the time of publication.